European Community on Computational Methods in Applied Sciences

ECCOMAS Congress 2016

VII European Congress

on Computational Methods in Applied Sciences and Engineering

PROCEEDINGS

Volume IV

M. Papadrakakis, V. Papadopoulos, G. Stefanou, V. Plevris (Eds)

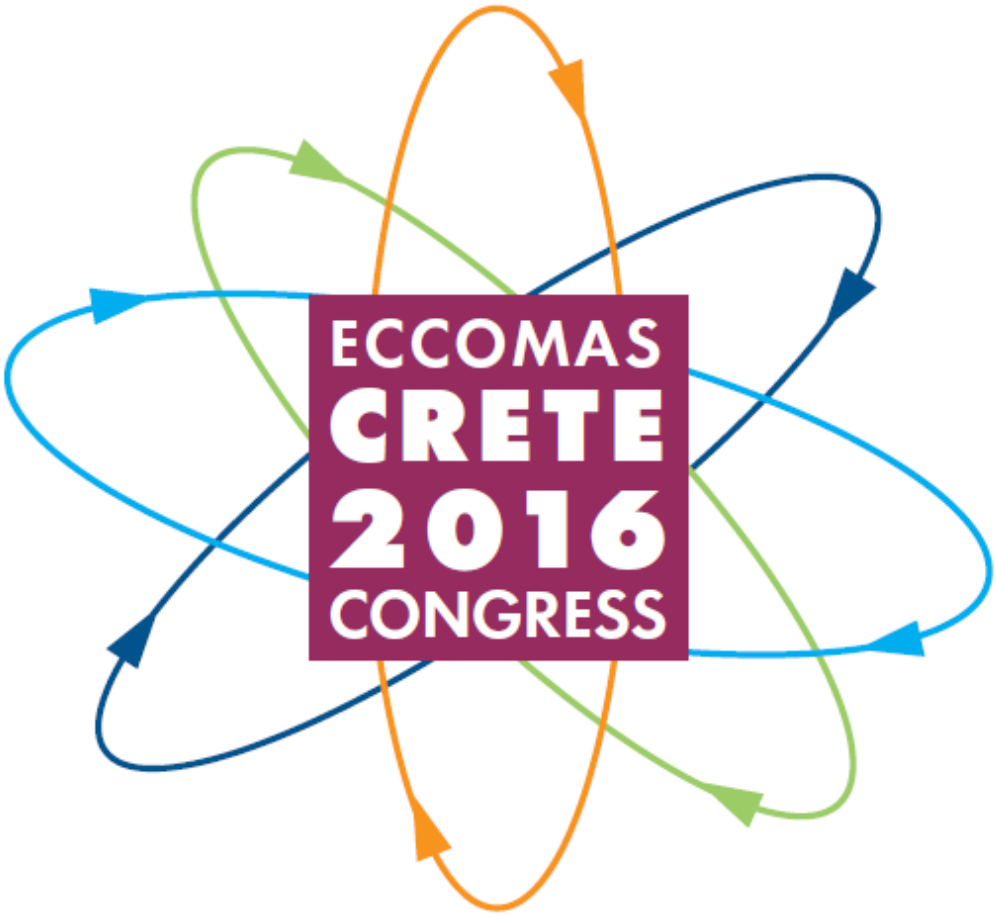

ECCOMAS Congress 2016

Proceedings of the VII European Congress on Computational Methods
in Applied Sciences and Engineering
Held in Crete, Greece
5-10 June 2016

Edited by:

M. Papadrakakis
National Technical University of Athens, Greece

V. Papadopoulos
National Technical University of Athens, Greece

G. Stefanou
Aristotle University of Thessaloniki, Greece

V. Plevris
Oslo and Akershus University College of Applied Sciences, Oslo, Norway

A publication of:

Institute of Structural Analysis and Antiseismic Research
School of Civil Engineering
National Technical University of Athens (NTUA)
Greece

ECCOMAS Congress 2016
M. Papadrakakis, V. Papadopoulos, G. Stefanou, V. Plevris (Eds)

First Edition, September 2016

ISBN: **978-618-82844-0-1**

ECCOMAS Congress 2016
VII European Congress on Computational Methods in Applied Sciences and Engineering
M. Papadrakakis, V. Papadopoulos, G. Stefanou, V. Plevris (eds.)
Crete Island, Greece, 5–10 June 2016

THREE-DIMENSIONAL BE–FE MODEL OF BUCKET FOUNDATIONS IN POROELASTIC SOILS

Jacob D. R. Bordón , Juan J. Aznárez, Orlando F. Maeso

Instituto Universitario de Sistemas Inteligentes y Aplicaciones Numricas en Ingeniera
Universidad de Las Palmas de Gran Canaria
Edificio Central del Parque Cientfico y Tecnolgico del Campus Universitario de Tafira, 35017 Las Palmas de Gran Canaria, Spain
e-mail: {jdrodriguez,jaznarez,omaeso}@iusiani.ulpgc.es

Keywords: bucket foundations, poroelasticity, impedances, Dual BEM, BEM–FEM coupling

Abstract. *A three-dimensional BE–FE model for the time harmonic analysis of bucket foundations in poroelastic soils is presented. The soil follows the Biot's poroelasticity and is discretized using the BEM. The skirt of the bucket is modeled as a degenerated shell finite element. The soil-structure interaction is taken into account assuming a crack-like boundary from the soil point of view, where the Dual BEM is applied. It is shown that this simple representation is accurate and efficient. This model is applied to an analysis of the impedances of bucket foundations, where the influences of the foundation geometry and soil properties are studied. The study shows that, when considering realistic seabed soils, a poroelastic model should be used for the low-frequency range (*$< 1 - 6$ Hz *depending on the seabed soil). It is shown that this is particularly true for bucket foundations with small length to diameter ratios.*

1 INTRODUCTION

Bucket foundations (or suction caisson foundations) are used as anchors and foundations of offshore platforms, and more recently as foundations of offshore wind turbines when suitable water depths and soil conditions are encountered [1]. Foundations of offshore wind turbines experience important horizontal and moment loadings, which are larger for deeper waters. Single bucket or monopod foundations are used for wind turbines installed at moderate water depths. When monopod foundations are not enough to carry these loads, three or four small buckets can be combined to form what are known as tripod or tetrapod foundations. In general, wind turbines with bucket foundations are well suited for water depths between 20 to 50 meters [2].

Despite the experience gained from oil and gas industries, their application to wind turbines faces several new challenges [1, 3]. They must be designed to withstand large horizontal forces and overturning moments, and in addition these are of dynamic nature. These loads mainly comes from steady-state operation of the machine (rotor rotation), wind field, water current field, water waves, tidal effects, and earthquakes. Furthermore, the installation process and the soil conditions of the seabed near the foundation introduce several uncertainties. These designs should be able to operate under such conditions for a number of years in order to be economically viable. Therefore, it is necessary to advance towards the development of rigorous models able to take into account realistic conditions.

Many aspects of the installation and design of bucket foundations have been studied, and the literature is large. A very complete review about bearing capacity and installation was published by Foglia and Ibsen [4]. In the context of dynamics, a recent work of Kourkoulis et al. [5] uses a non-linear FEM model to study the behaviour of bucket foundations of offshore wind turbines under lateral monotonic, cyclic, and earthquake loading. They give an interesting discussion about the interface conditions between soil and foundation. Liingaard et al. [6] studied the impedances of bucket foundations in elastic soils, including the variation of these under changes of geometry and soil properties.

In the present work, dynamic stiffnesses of bucket foundations buried in poroelastic soils are studied. A simple but accurate boundary element – finite element (BE–FE) model is developed to this aim. Bucket foundations with different skirt length to diameter ratios buried in different realistic seabed soils are considered. Also, the effect of different contact conditions between the lid and the seabed is studied.

The rest of the paper is organized as follows. In Section 2, the boundary element – finite element model is described. In Section 3, impedances of bucket foundations buried in different poroelastic seabeds are obtained and discussed. Finally, in Section 4 the main conclusions are given.

2 BE–FE MODEL

2.1 Conventional and Dual BEM for three-dimensional Biot's poroelasticity

The soil is considered to be a homogeneous poroelastic half-space following the Biot's theory of poroelasticity. Given its unbounded nature, the BEM is used to numerically treat it. A particular feature of the proposed model is that, unlike Liingaard et al. [6], the problem can be handled directly without needing any artificial interfaces. This is achieved thanks to the usage of the Dual BEM.

The governing equations of Biot's poroelasticity [7] in the time domain can be written as:

$$\mu\boldsymbol{\nabla}^2\mathbf{u}+\boldsymbol{\nabla}\left[\left(\lambda+\mu+Q^2/R\right)(\boldsymbol{\nabla}\cdot\mathbf{u})+Q\,(\boldsymbol{\nabla}\cdot\mathbf{U})\right]+\mathbf{X}=\rho_{11}\ddot{\mathbf{u}}+\rho_{12}\ddot{\mathbf{U}}+b\left(\dot{\mathbf{u}}-\dot{\mathbf{U}}\right) \quad (1)$$

$$\boldsymbol{\nabla}\left[Q\,(\boldsymbol{\nabla}\cdot\mathbf{u})+R\,(\boldsymbol{\nabla}\cdot\mathbf{U})\right]+\mathbf{X}'=\rho_{12}\ddot{\mathbf{u}}+\rho_{22}\ddot{\mathbf{U}}-b\left(\dot{\mathbf{u}}-\dot{\mathbf{U}}\right) \quad (2)$$

and the stress-strain relationships are:

$$\tau_{ij}=\delta_{ij}\left[\left(\lambda+Q^2/R\right)(\boldsymbol{\nabla}\cdot\mathbf{u})+Q\,(\boldsymbol{\nabla}\cdot\mathbf{U})\right]+\mu\left(u_{i,j}+u_{j,i}\right),\quad i,j=1,2,3 \quad (3)$$

$$\tau=Q\,(\boldsymbol{\nabla}\cdot\mathbf{u})+R\,(\boldsymbol{\nabla}\cdot\mathbf{U}) \quad (4)$$

where u_i, τ_{ij} and $\mathbf{X}$ are respectively displacements, stresses and body forces in the solid phase, and U_i, τ and $\mathbf{X}'$ are respectively displacements, equivalent stress and body forces in the fluid phase. The poroelastic medium has the following properties: λ and μ are the Lamé's parameters of the solid phase, Q and R are the Biot's coupling parameters, b is the dissipation constant, and $\rho_{11}=(1-\phi)\rho_{\mathrm{s}}+\rho_{\mathrm{a}}$, $\rho_{12}=-\rho_{\mathrm{a}}$, $\rho_{22}=\phi\rho_{\mathrm{f}}+\rho_{\mathrm{a}}$, being ϕ the porosity, ρ_{s} the solid phase density, ρ_{f} the fluid phase density, and ρ_{a} the additional apparent density. The additional apparent density ρ_{a} is obtained from $\rho_{\mathrm{a}}=(\alpha-1)\phi\rho_{\mathrm{f}}$, where α is the tortuosity [8]. The dissipation constant b is related to the hydraulic conductivity k by the relationship $b=\rho_{\mathrm{f}}g\phi^2/k$, where g is the gravitational acceleration [9]. In the frequency domain ω, Equations (1-2) can be written as:

$$\mu\boldsymbol{\nabla}^2\mathbf{u}+\boldsymbol{\nabla}\left[\left(\lambda+\mu+Q^2/R\right)(\boldsymbol{\nabla}\cdot\mathbf{u})+Q\,(\boldsymbol{\nabla}\cdot\mathbf{U})\right]+\mathbf{X}=-\omega^2\hat{\rho}_{11}\mathbf{u}-\omega^2\hat{\rho}_{12}\mathbf{U} \quad (5)$$

$$\boldsymbol{\nabla}\left[Q\,(\boldsymbol{\nabla}\cdot\mathbf{u})+R\,(\boldsymbol{\nabla}\cdot\mathbf{U})\right]+\mathbf{X}'=-\omega^2\hat{\rho}_{12}\mathbf{u}-\omega^2\hat{\rho}_{22}\mathbf{U} \quad (6)$$

where $\hat{\rho}_{11}=\rho_{11}-ib/\omega$, $\hat{\rho}_{22}=\rho_{22}-ib/\omega$ and $\hat{\rho}_{12}=\rho_{12}+ib/\omega$. It is well known that three bulk modes exists: two longitudinal modes (P1 and P2) and one transverse mode (S); and their associated wavenumbers are denoted respectively as k_1, k_2 and k_3.

The BEM is based on the usage of Boundary Integral Equations (BIE), which are used to build a solvable linear system of equations after its discretization. Domínguez [10, 11] presented a BEM based on a Singular BIE (SBIE) for two-dimensional Biot's poroelasticity, and Maeso et al. [12] extended it to three-dimensions. One of the advantages of this family of BIEs over others is the reduction of the variables related to the fluid phase to two: the equivalent stress τ and the normal displacement U_n. Another advantage is the possibility of writing the fundamental solution and its derivatives in a way that resembles the fundamental solutions of acoustics and elastodynamics and their derivatives.

Let Ω be a poroelastic region, and $\Gamma=\partial\Omega$ its boundary with outward unit normal $\mathbf{n}$. Using the weighted residual formulation proposed by Domínguez [10, 12], the SBIE at a collocation point $\mathbf{x}^{\mathrm{i}}$ can be written as:

$$\begin{bmatrix} Jc^{\mathrm{i}} & 0 \\ 0 & c^{\mathrm{i}}_{lk}\end{bmatrix}\begin{Bmatrix}\tau^{\mathrm{i}}\\ u^{\mathrm{i}}_k\end{Bmatrix}+\oint_\Gamma\begin{bmatrix}-(U^*_{n00}+JX'^*_j n_j)\,t^*_{0k} \\ -U^*_{nl0} \qquad\qquad t^*_{lk}\end{bmatrix}\begin{Bmatrix}\tau\\ u_k\end{Bmatrix}\mathrm{d}\Gamma=\int_\Gamma\begin{bmatrix}-\tau^*_{00} & u^*_{0k}\\ -\tau^*_{l0} & u^*_{lk}\end{bmatrix}\begin{Bmatrix}U_n\\ t_k\end{Bmatrix}\mathrm{d}\Gamma$$

$$\mathbf{C}^{\mathrm{i}}_{\mathrm{S}}\mathbf{u}^{\mathrm{i}}+\oint_\Gamma\mathbf{T}^*\mathbf{u}\,\mathrm{d}\Gamma=\int_\Gamma\mathbf{U}^*\mathbf{t}\,\mathrm{d}\Gamma \quad (7)$$

where $l,k=1,2,3$, and $J=1/(\hat{\rho}_{22}\omega^2)$. The vector $\mathbf{u}$ contains the primary variables: fluid equivalent stress τ and solid displacements u_k; and $\mathbf{t}$ contains the secondary variables: fluid normal displacement $U_n=U_jn_j$ and solid traction $t_k=\tau_{kj}n_j$. The superscript $\square^{\mathrm{i}}$ is not an

index, and indicates that the corresponding variable is related to the collocation point. The free-term matrix $\mathbf{C}^{\mathrm{i}}_{\mathrm{S}}$ contains the potential free-term c^{i} and the elastostatic free-term c^{i}_{lk}, which are $c^{\mathrm{i}} = 1$ and $c^{\mathrm{i}}_{lk} = \delta_{lk}$ for an interior collocation point ($\mathbf{x}^{\mathrm{i}} \in \Omega$), and $c^{\mathrm{i}} = 1/2$ and $c^{\mathrm{i}}_{lk} = 1/2\delta_{lk}$ for a smooth boundary collocation point ($\mathbf{x}^{\mathrm{i}} \in \Gamma$, $\Gamma(\mathbf{x}^{\mathrm{i}}) \in \mathcal{C}^1$). As usual, the notation $\oint$ stands for an integral in the Cauchy Principal Value (CPV) sense, which is evaluated as described in [12].

The Hypersingular BIE (HBIE) for two-dimensional problems was obtained by Bordón et al. [13]. Likewise, the three-dimensional HBIE is built by establishing the secondary variables at the collocation point:

$$U^{\mathrm{i}}_n = U^{\mathrm{i}}_j n^{\mathrm{i}}_j = -J\tau^{\mathrm{i}}_{,j} n^{\mathrm{i}}_j - Z u^{\mathrm{i}}_j n^{\mathrm{i}}_j \tag{8}$$

$$t^{\mathrm{i}}_l = \tau^{\mathrm{i}}_{lj} n^{\mathrm{i}}_j = \left[\lambda u^{\mathrm{i}}_{m,m}\delta_{lj} + \mu\left(u^{\mathrm{i}}_{l,j} + u^{\mathrm{i}}_{j,l}\right)\right] n^{\mathrm{i}}_j + \frac{Q}{R}\tau^{\mathrm{i}} n^{\mathrm{i}}_l \tag{9}$$

where $Z = \hat{\rho}_{12}/\hat{\rho}_{22}$, $\mathbf{n}^{\mathrm{i}}$ is the unit normal vector at the collocation point, and the comma derivative notation denotes $\partial/\partial x^{\mathrm{i}}_k$. Therefore, a mix of the SBIE and its derivatives with respect to the collocation point is required to build the HBIE. After carrying out all the required operations, the HBIE at a collocation point $\mathbf{x}^{\mathrm{i}}$ with unit normal $\mathbf{n}^{\mathrm{i}}$ can be written as:

$$\begin{gathered}\begin{bmatrix} c^{\mathrm{i}} & 0 \\ 0 & c^{\mathrm{i}}_{lk} \end{bmatrix} \begin{Bmatrix} U^{\mathrm{i}}_n \\ t^{\mathrm{i}}_k \end{Bmatrix} + \fint_\Gamma \begin{bmatrix} -s^*_{00} & s^*_{0k} \\ -s^*_{l0} & s^*_{lk} \end{bmatrix} \begin{Bmatrix} \tau \\ u_k \end{Bmatrix} \mathrm{d}\Gamma = \oint_\Gamma \begin{bmatrix} -d^*_{00} & d^*_{0k} \\ -d^*_{l0} & d^*_{lk} \end{bmatrix} \begin{Bmatrix} U_n \\ t_k \end{Bmatrix} \mathrm{d}\Gamma \\ \mathbf{C}^{\mathrm{i}}_{\mathrm{H}}\mathbf{t}^{\mathrm{i}} + \fint_\Gamma \mathbf{S}^*\mathbf{u}\,\mathrm{d}\Gamma = \oint_\Gamma \mathbf{D}^*\mathbf{t}\,\mathrm{d}\Gamma\end{gathered} \tag{10}$$

where the notation $\fint$ stands for an integral in the Hadamard Finite Part (HFP) sense. The presence of a HFP integral imposes that the primary variables at the collocation point must have continuous first derivatives, i.e. $\tau(\mathbf{x}^{\mathrm{i}}),\ u_k(\mathbf{x}^{\mathrm{i}}) \in \mathcal{C}^1$. Using this fact, a meaningful HBIE can be obtained once a regularization process based on the work of Domínguez et al. [14] is performed.

Equations (7) and (10) correspond to BIEs for interior collocation points, or boundary collocation points at ordinary boundaries. When the collocation point is located at a crack-like boundary, both BIEs have to be modified. A crack-like boundary has two boundaries geometrically coincident but with opposite orientations, denoted as positive $+$ and negative $-$ faces. Hence, the SBIE and HBIE when the collocation point $\mathbf{x}^{\mathrm{i}}$ is located at a crack-like boundary can be written as:

$$\frac{1}{2}\begin{bmatrix} J & 0 \\ 0 & \delta_{lk} \end{bmatrix} \left(\mathbf{u}^{\mathrm{i}+} + \mathbf{u}^{\mathrm{i}-}\right) + \oint_\Gamma \mathbf{T}^*\mathbf{u}\,\mathrm{d}\Gamma = \int_\Gamma \mathbf{U}^*\mathbf{t}\,\mathrm{d}\Gamma \tag{11}$$

$$\frac{1}{2}\begin{bmatrix} 1 & 0 \\ 0 & \delta_{lk} \end{bmatrix} \left(\mathbf{t}^{\mathrm{i}+} - \mathbf{t}^{\mathrm{i}-}\right) + \fint_\Gamma \mathbf{S}^*\mathbf{u}\,\mathrm{d}\Gamma = \oint_\Gamma \mathbf{D}^*\mathbf{t}\,\mathrm{d}\Gamma \tag{12}$$

where it has been assumed that $\Gamma(\mathbf{x}^{\mathrm{i}}) \in \mathcal{C}^1$. Both Equations (11) and (12) have to be used simultaneously in order to solve problems where crack-like boundaries are present. When considered this way, they are known as Dual BIEs, and their application to the BEM is called the Dual BEM [15, 16]. As explained before, the HBIE requires that $\tau(\mathbf{x}^{\mathrm{i}}),\ u_k(\mathbf{x}^{\mathrm{i}}) \in \mathcal{C}^1$, thus the collocation at crack-like boundaries must be performed carefully. Aliabadi and co-workers [15, 16] use discontinuous boundary elements with nodes already located at points where this condition is fulfilled. Another approach is that of Domínguez et al. [14], where standard continuous boundary elements with multiple non-nodal collocation is used. The latter is considered in the present work since, as it will become clear in the next section, continuous boundary elements are much more appropriate for the proposed coupling.

2.2 Degenerated shell finite element

The bucket foundation is considered to be a massless linear elastic solid. It is modelled with degenerated shell finite elements. The degenerated shell FE has been formulated and implemented following Oñate [17], and a robust 8-noded quadrilateral element with reduced integration is used.

2.3 BE–FE coupling

The BE–FE coupling is done at the level of discretized equations. The boundary element mesh and the finite element mesh must be conforming. A perfect bonding between the mid-surface of the shell and the crack-like boundary of the soil is considered. It means that rotations are not taken into account in the coupling. Given the small thickness to length ratio of the bucket skirt, their contribution can be neglected. Furthermore, since the bucket is made of steel, an impermeable interface between the shell and the poroelastic soil is assumed.

Consider n_j^+, U_n^+, u_i^+, τ^+ and t_i^+ as respectively the unit normal, fluid normal displacement, solid displacement, fluid equivalent stress and solid traction of the positive face of the crack-like boundary (soil), and analogously for the negative face. Also, consider u_i^{s} as the displacement of the mid-surface, and t_i^{s} as the distributed load on the mid-surface. Then, the compatibility and equilibrium coupling conditions between the crack-like boundary and the mid-surface of the shell can be written as:

$$U_n^+ = u_j^+ n_j^+,\ U_n^- = u_j^- n_j^-,\ u_i^+ = u_i^{\mathrm{s}},\ u_i^- = u_i^{\mathrm{s}} \tag{13}$$

$$\tau^+ n_i^+ + t_i^+ + \tau^- n_i^- + t_i^- + t_i^{\mathrm{s}} = 0 \tag{14}$$

3 IMPEDANCES OF BUCKET FOUNDATIONS

A bucket foundation is composed of a rigid lid with diameter D, and a flexible skirt of length L and thickness t. Using six degrees of freedom at the center of the lid, it is possible to build an impedance matrix $\mathbf{S}$ relating the forces and moments $\mathbf{R}$ produced by unitary displacements and rotations $\mathbf{U}$. Since buckets are axisymmetric, the impedance matrix has five different impedance functions: horizontal (S_{HH}), vertical (S_{VV}), rocking (S_{MM}), horizontal-rocking coupling (S_{MH}), and torsional (S_{TT}). In the present paper, all impedance functions are studied except the torsional one. For the sake of brevity, the same notation and normalization procedure as Liingaard et al. [6] is used.

Elastic soils can be defined by a small set of properties, for example shear modulus μ, Poisson's ratio ν, density ρ and a hysteretic damping ratio ξ ($\mu^* = \mu(1 + i2\xi)$). Hence, fully dimensionless studies can be carried out by defining some shape factors of the structure, a dimensionless frequency a_0 with the help of a length of the structure and a wave velocity of the soil, and setting the Poisson's ratio and damping ratio of the soil. In the case of poroelastic soils, this task becomes impractical due to the number of properties involved, and the difficulties of knowing if a given set of values of the properties represents a realistic soil or not. For these reasons, we have decided to use realistic seabed soils taken from Buchanan and Gilbert [18], see Table 1. All results are shown using a dimensionless frequency $a_0 = \omega R/c_{\mathrm{S}}^{\mathrm{u}}$, where R is the radius of the bucket, and $c_{\mathrm{S}}^{\mathrm{u}} = \sqrt{\mu/(\phi\rho_{\mathrm{f}} + (1-\phi)\rho_{\mathrm{s}})}$ is the undrained S-wave velocity.

The bucket foundation is considered massless ($\rho = 0\ \mathrm{kg/m^3}$), with a Young's modulus $E = 210\ \mathrm{GPa}$, Poisson's ratio $\nu = 1/4$ and hysteretic damping ratio $\xi = 0.01$ ($E^* = E(1 + i2\xi)$). The diameter is $D = 10\ \mathrm{m}$, and the thickness $t = 0.05\ \mathrm{m}$. Because of the nature of the BE-FE coupling presented, the mass distribution through the soil-structure interface is continuous according to the density of the soil despite the structure is considered massless.

Property, symbol and units	**Coarse sand and fine gravel (sb1)**	**Coarse sand (sb2)**	**Fine sand (sb3)**	**Silty clay (sb4)**	**Silty sand (sb5)**
Frame shear modulus $\mathrm{Re}\,(\mu^*)$ [MPa]	12.50	74.00	7.12	0.79	41.00
Frame shear modulus $\mathrm{Im}\,(\mu^*)$ [MPa]	4.50	4.70	0.23	0.03	7.90
Frame bulk modulus $\mathrm{Re}\,(K^*)$ [MPa]	27.10	52.00	9.49	3.67	29.00
Frame bulk modulus $\mathrm{Im}\,(K^*)$ [MPa]	0.90	0.74	0.30	0.12	1.30
Poisson's ratio ν [–]	0.30	0.02	0.20	0.40	0.02
Porosity ϕ [–]	0.30	0.38	0.43	0.68	0.65
Fluid bulk modulus K_f [GPa]	2.38	2.40	2.39	2.38	2.40
Biot's coupling paramater Q [GPa]	1.666	1.488	1.362	0.762	0.840
Biot's coupling paramater R [GPa]	0.714	0.912	1.028	1.618	1.560
Fluid density ρ_f [kg/m^3]	1000	1000	1000	1000	1000
Solid density ρ_s [kg/m^3]	2680	2710	2670	2680	2670
Tortuosity α [–]	1.25	1.25	1.25	3.00	3.00
Additional apparent den. ρ_a [kg/m^3]	75	95	107.5	1360	1300
Fluid viscosity η [mPa $\cdot$ s]	1.01	1.01	1.01	1.01	1.01
Permeability κ [m^2]	$2.6 \cdot 10^{-10}$	$7.5 \cdot 10^{-11}$	$3.1 \cdot 10^{-14}$	$5.2 \cdot 10^{-14}$	$6.3 \cdot 10^{-15}$
Hydraulic conductivity k [m/s]	$2.5 \cdot 10^{-3}$	$7.3 \cdot 10^{-4}$	$3.0 \cdot 10^{-7}$	$5.1 \cdot 10^{-7}$	$6.2 \cdot 10^{-8}$
Disipation constant b [N $\cdot$ s/m^4]	$3.52 \cdot 10^{5}$	$1.95 \cdot 10^{6}$	$5.99 \cdot 10^{9}$	$8.98 \cdot 10^{9}$	$6.74 \cdot 10^{10}$
Undrained Poisson's ratio ν^u [–]	0.4992153	0.4942119	0.4993609	0.4998878	0.4945113
Bulk density ρ [kg/m^3]	2176	2060	1952	1538	1585
Undrained S-wave velocity c_S^u [m/s]	75.8	189.5	60.4	22.6	160.9

Table 1: Properties of seabed soils taken from Buchanan [18]. Top: poroelastic medium. Bottom: undrained solid.

Impedances are calculated using a BE-FE model based on the methodology described in the previous section. Figure 1 shows a mesh used in the calculations. Taking into account the symmetric nature of the geometry, only one-quarter of the domain is discretized. The soil region Ω_soil has three BE boundaries: the seabed free-surface $\Gamma_{\mathrm{free-surface}}$, the soil-skirt interface $\Gamma_{\mathrm{soil-skirt}}$ (a crack-like boundary), and the bucket lid Γ_lid. The skirt region Ω_skirt is a mesh of degenerated shell FE. For the sake of clarity in Figure 1, the skirt Ω_skirt is not located at its real position, which is exactly in the position of $\Gamma_{\mathrm{soil-skirt}}$. The seabed free-surface $\Gamma_{\mathrm{free-surface}}$ is a permeable traction-free boundary, i.e. $\tau = 0$ and $t_k = 0$. The bucket lid Γ_lid has prescribed fluid and solid displacements according to the impedance that is being being calculated. Shell FE nodes in ($x > 0$, $y > 0$, $z = 0$) and in zx and yz symmetry planes are 6 DOF shell nodes, while the rest are 5 DOF nodes. By doing so, it is easy to establish the prescribed displacements and rotations to the 6 DOF nodes according to the impedance that is being calculated and the symmetric/anti-symmetric conditions imposed by the displacement field. Both $\Gamma_{\mathrm{soil-skirt}}$ and Ω_skirt are discretized with conforming meshes of 8-noded quadrilateral elements. Boundaries Γ_lid and $\Gamma_{\mathrm{free-surface}}$ are discretized with 6-noded triangular elements. The size of the elements of the foundation and its surroundings is at least of 6 elements per wavelength, while at least 4 elements per wavelength is used beyond it.

3.1 Validation

In order to check the validity of the formulation and the models, a comparison between several results of Liingaard et al. [6] and results from our BE-FE model is done. Figure 2 shows impedances (normalized magnitude and angle) for bucket foundations with several length to diameter ratios $L/D = \{1/4, 1, 2\}$. The given elastic soil properties are $\mu = 1$ MPa, $\nu = 1/3$

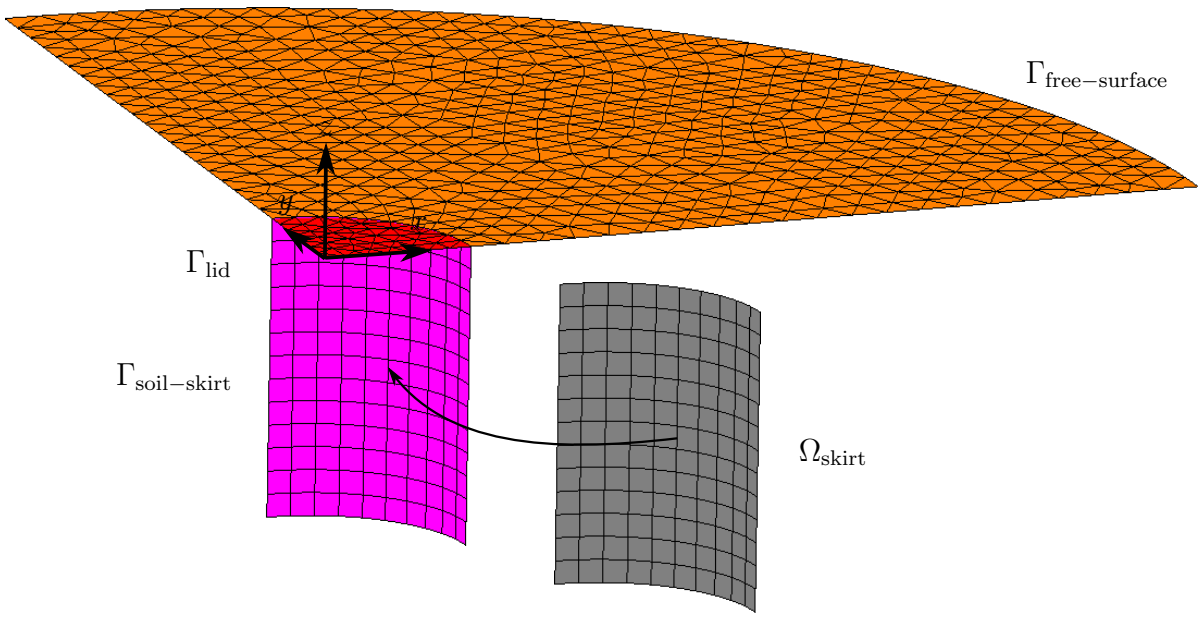

Figure 1: Description of a mesh used in the calculations ($L/D = 1$)

and $\xi = 0.025$. In our model, the same properties are used for the solid, the fluid is considered to be air, and a small porosity is used $\phi \to 0$. Figure 2 demonstrates complete agreement between results. Although not shown here, all other static and dynamic results presented in [6] also agree with results obtained by our model.

3.2 Results and discussion

Seabed soils taken from Buchanan and Gilbert [18], see Table 1, cover a wide range of possible realistic soils, from gravels, sands, silts, to clays. These soils are denoted as "sb1" to "sb5" in the following tables and graphs. Three length to diameter ratios $L/D = \{1/4, 1, 2\}$ are studied. Table 2 shows the dimensionless quasi-static stiffnesses for all cases, where they are calculated for a small dimensionless frequency $a_0 = 10^{-6}$. Nondimensionalization of impedances is performed using the shear modulus μ of the soil and the radius R of the bucket. Figures 3 to 5 show the impedances for all cases, where in the low-frequency range ($a_0 = [10^{-6}, 1]$) only their magnitudes are analysed, and in a broader frequency range ($a_0 = [0, 6]$) also their angles are shown. Taking into account the definition of the dimensionless frequency a_0, the low-frequency range corresponds approximately to frequencies below $1 - 6$ Hz depending on the seabed soil. Also, the broader frequency range corresponds approximately to frequencies between $1 - 6$ Hz and 40 Hz depending on the seabed soil.

Dimensionless quasi-static stiffnesses are similar in magnitude to those obtained by Liingaard et al [6] for elastic soils, considering the seabed as a drained elastic soil. In fact, Table 2 includes the results using an elastic solid with the drained conditions of the porous medium, and the discrepancy is small. Differences are due to a not sufficiently small dimensionless frequency for the calculation of the quasi-static stiffness.

As can be seen in the left hand side graphs of Figures 3 to 5, impedance functions are almost constant and approximately equal to the quasi-static value in the low-frequency range. This is characteristic of any elastic soil, which is even more smooth. In the case of poroelastic soils, the smaller length to diameter ratio the less regular behaviour at low-frequencies. In the case of buckets with $L/D = 1/4$, it is very noticeable the variation of impedances when $a_0 \to 0$.

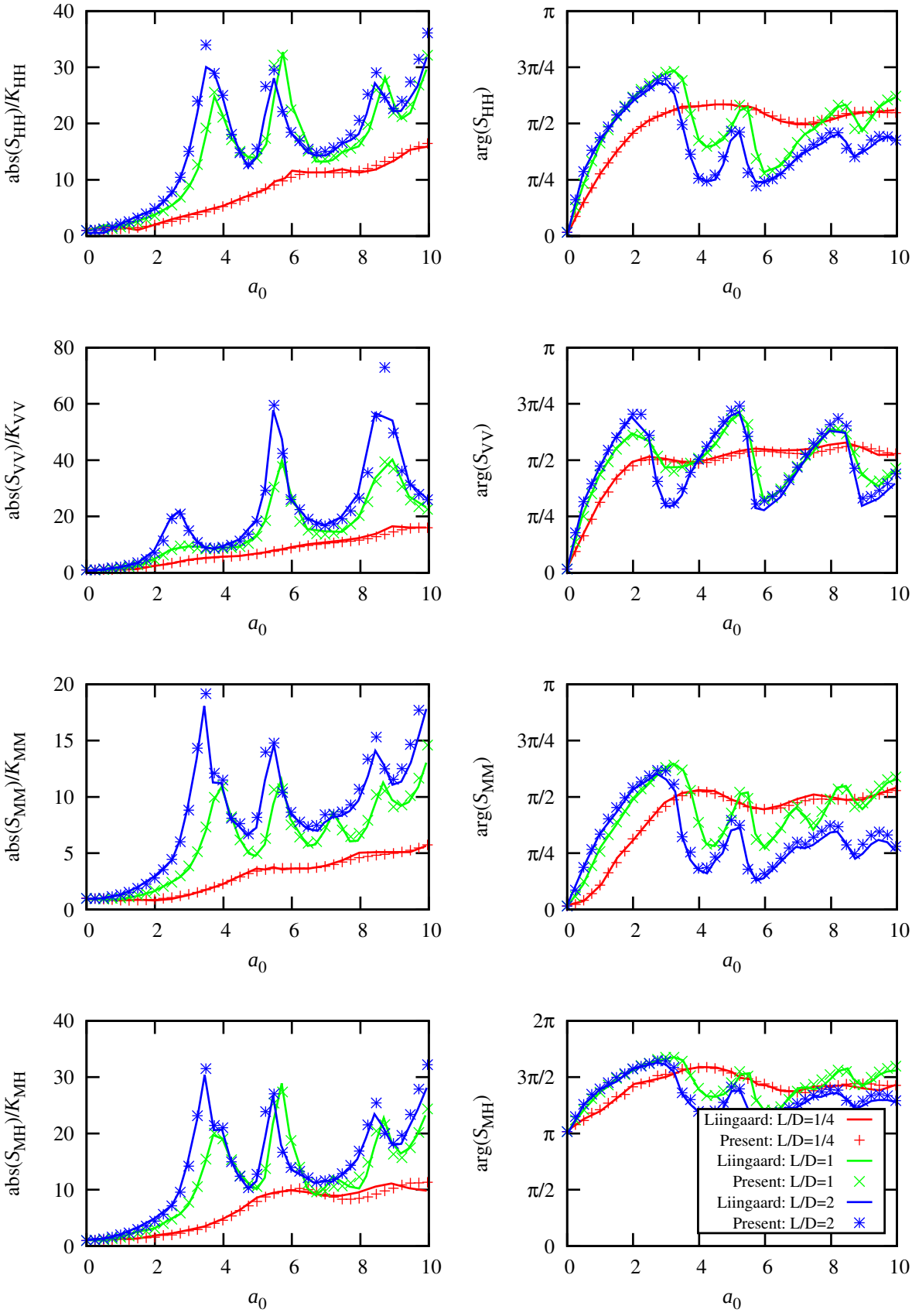

Figure 2: Comparison between Liingaard et al. [6] and the present approach. From top to bottom: normalized horizontal, vertical, rocking, and horizontal-rocking coupling impedances.

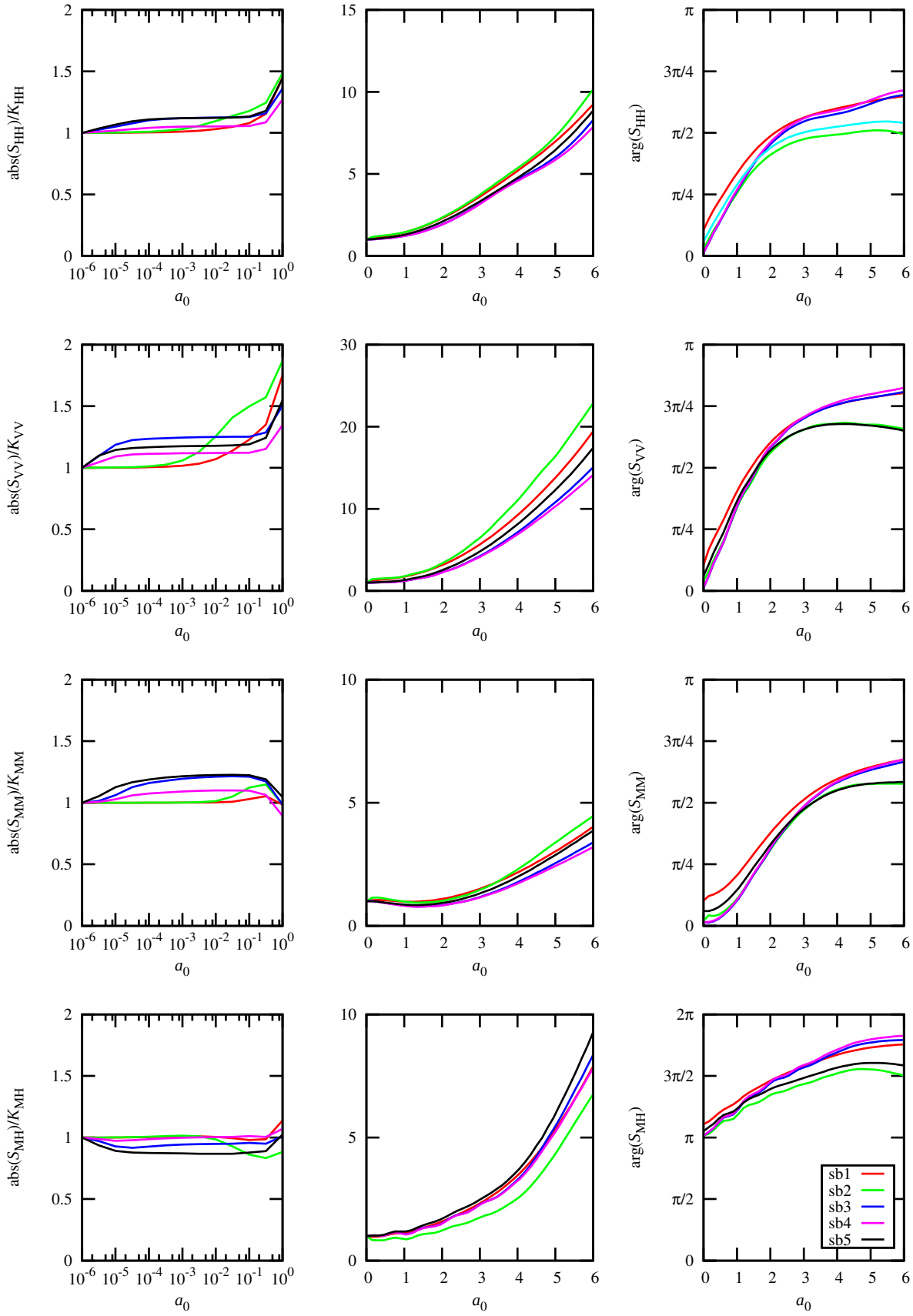

Figure 3: Impedances of bucket foundations with $L/D = 1/4$ in poroelastic soils. From top to bottom: horizontal, vertical, rocking, and horizontal-rocking coupling impedances normalized with respect to the corresponding quasi-static stiffness.

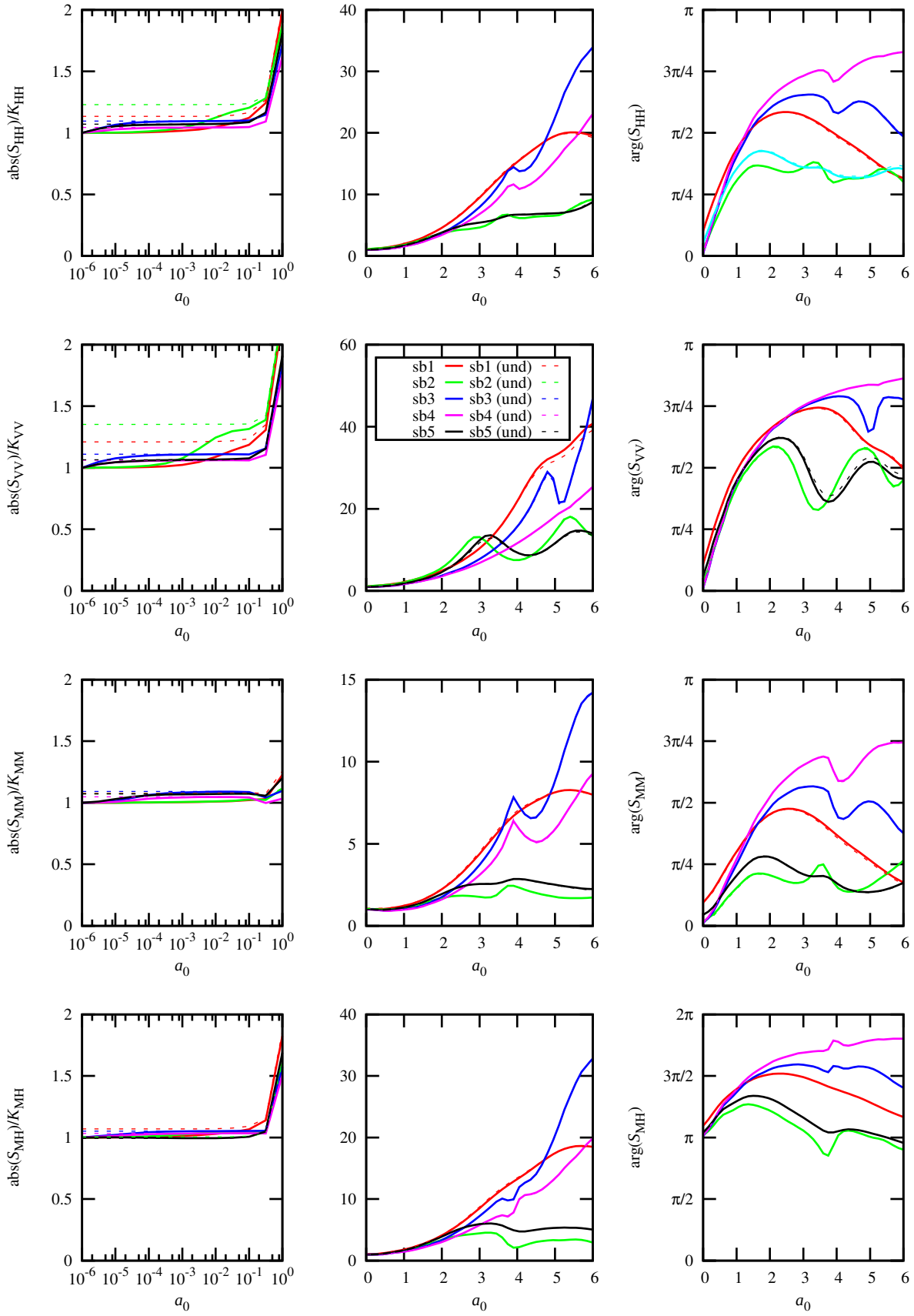

Figure 4: Impedances of bucket foundations with $L/D = 1$ in poroelastic soils and corresponding undrained elastic soils (dashed lines) . From top to bottom: horizontal, vertical, rocking, and horizontal-rocking coupling impedances normalized with respect to the corresponding quasi-static stiffness using the poroelastic soil.

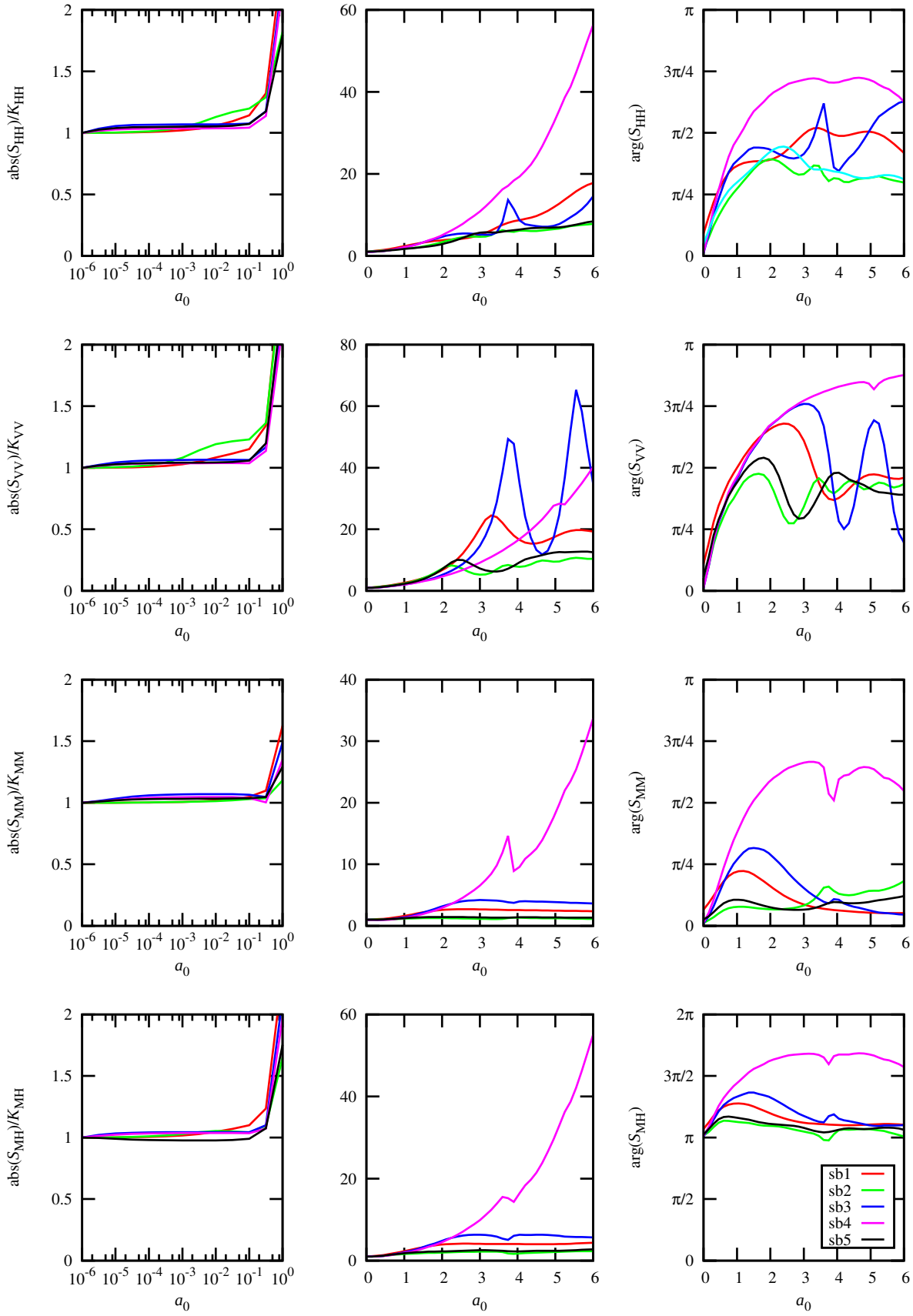

Figure 5: Impedances of bucket foundations with $L/D = 2$ in poroelastic soils. From top to bottom: horizontal, vertical, rocking, and horizontal-rocking coupling impedances normalized with respect to the corresponding quasi-static stiffness.

Quasi-static stiffness (porous: $a_0 = 10^{-6}$)	**Seabed soil**	$\frac{L}{D} = \frac{1}{4}$	$\frac{L}{D} = 1$		$\frac{L}{D} = 2$
		Porous	Porous	Drained	Porous
K_{HH}	sb1	7.774	13.073	13.116 (0.3%)	16.137
	sb2	6.186	8.900	8.892 (0.1%)	9.385
	sb3	7.445	13.198	12.175 (7.8%)	17.754
	sb4	8.065	14.516	14.069 (3.1%)	21.614
	sb5	7.216	11.525	9.956 (13.6%)	12.723
K_{VV}	sb1	7.557	11.288	11.336 (0.4%)	15.502
	sb2	5.822	8.954	8.946 (0.1%)	11.952
	sb3	7.483	11.662	10.124 (13.2%)	16.013
	sb4	8.403	12.321	11.58 (6.0%)	16.731
	sb5	7.904	11.849	9.283 (21.7%)	15.407
K_{MM}	sb1	8.739	47.368	47.48 (0.2%)	131.429
	sb2	7.066	28.100	28.096 (0.0%)	44.571
	sb3	8.003	46.973	46.246 (1.5%)	153.538
	sb4	8.993	53.106	52.728 (0.7%)	217.156
	sb5	7.581	35.139	34.53 (1.7%)	68.016
K_{MH}	sb1	−2.778	−15.539	−15.572 (0.2%)	−30.881
	sb2	−2.464	−8.816	−8.806 (0.1%)	−10.950
	sb3	−2.729	−16.036	−15.307 (4.5%)	−37.250
	sb4	−2.700	−17.923	−17.561 (2.0%)	−51.545
	sb5	−2.550	−11.751	−11.112 (5.4%)	−17.182

Table 2: Quasi-static stiffnesses of the studied bucket foundations and seabed soils

The effect is due to the permeability of the porous medium, the smaller permeability the more pronounced variation. It is more relevant for buckets with smaller length to diameter ratios because of the relevance of the compressional interaction of the bucket lid with respect to the total impedance.

In Figure 4, results of the corresponding undrained elastic soils are included, and they are normalized with respect to the quasi-static stiffnesses of the correspoding porous media. Along the low-frequency range (except when $a_0 \to 0$), it is quite clear that neither the drained nor the undrained elastic soil is able to reproduce the real poroelastic behaviour.

The right hand side and central graphs of Figures 3 to 5 show impedance functions for a broader frequency range ($a_0 = [0, 6]$). By comparing these graphs and those obtained by Liingaard et al. [6] for elastic soils, the same qualitative behaviour is observed. For small length to diameter ratios, results tend to the solution of a disc foundation, while for larger ratios results tend to the solution of an infinite hollow cylinder. As shown in Figure 4, the behaviour is not only qualitatively similar, but also numerically if the corresponding undrained elastic soil is used. The difference between the real poroelastic soil and the undrained elastic soil is very small.

4 CONCLUSIONS

In this paper, a simple, efficient and accurate three-dimensional BE-FE dynamic model able to directly manage bucket foundations in poroelastic soils is presented. The model makes use of the Dual Boundary Element Method in order to avoid using any artificial boundary in the discretization when thin open structures are buried in soils.

In this work, results of impedance functions for horizontal, vertical, rocking and horizontal-rocking coupling modes of bucket foundations buried in poroelastic soils are presented. A

realistic set of seabed soils are used to obtain the impedances. It is shown that the poroelastic nature of the seabed soil should be considered when studying a problem in the low-frequency range ($< 1-6$ Hz depending on the seabed soil). This is particularly true for bucket foundations with small length to diameter ratios.

ACKNOWLEDGEMENTS

This work was supported by the Subdirección General de Proyectos de Investigación of the Ministerio de Economía y Competitividad (MINECO) of Spain and FEDER through Research Project BIA2014-57640-R and also by the Agencia Canaria de Investigación, Innovación y Sociedad de la Información (ACIISI) of the Government of the Canary Islands and FEDER through Research Project ProID20100224. J.D.R. Bordón is recipient of the research fellowship FPU13/01224 from the Ministry of Education, Culture and Sports of Spain. The authors are grateful for this support.

REFERENCES

[1] G.T. Houlsby, B.W. Byrne, Suction caisson foundations for offshore wind turbines and anemometer masts. *Wind Engineering*, **24**, 249–255, 2000.

[2] Det Norske Veritas, *Design of offshore wind turbine structures*. Offshore Standard DNV-OS-J101, 2010.

[3] G.T. Houlsby, L.B. Ibsen, B.W. Byrne, Suction caissons for wind turbines. S. Gourvenec, M. Cassidy eds. *Frontiers in Offshore Geotechnics: ISFOG2005*, Perth, September 19-21 2005.

[4] A. Foglia, L.B. Ibsen, Bucket foundations: a literature review. *Department of Civil Engineering, Aalborg University*, DCE Technical Reports No **176**, 2014.

[5] R.S. Kourkoulis, P.C. Lekkakis, F.M. Gelagoti, A.M. Kaynia, Suction caisson foundations for offshore wind turbines subjected to wave and earthquake loading: effect of soil–foundation interface. *Géotechnique*, **64**, 171–185, 2014.

[6] M. Liingaard, L. Andersen, L.B. Ibsen, Impedance of flexible suction caissons. *Earthquake Engineering and Structural Dynamics*, **36**, 2249–2271, 2007.

[7] M.A. Biot, Theory of propagation of elastic waves in a fluid-saturated porous solid. I. Low-frequency range. *Journal of Acoustical Society of America*, **28**, 168–178, 1956.

[8] J.G. Berryman, Confirmation of Biot's theory. *Applied Physics Letters*, **37**, 382-384, 1980.

[9] S. Bougacha, J.L. Tassoulas, Seismic analysis of gravity dams I: modeling of sediments. *Journal of Engineering Mechanics*, **117**, 1826–1837, 1991.

[10] J. Domínguez, An integral formulation for dynamic poroelasticity. *Journal of Applied Mechanics*, **58**, 588–591, 1991.

[11] J. Domínguez, Boundary element approach for dynamic poroelastic problems. *International Journal for Numerical Methods in Engineering*, **35**, 307–324, 1992.

[12] O. Maeso and J.J. Aznárez and F. García, Dynamic impedances of piles and groups of piles in saturated soils. *Computers and Structures*, **83**, 769–782, 2005.

[13] J.D.R. Bordón, J.J. Aznárez, O. Maeso, Two-dimensional numerical approach for the vibration isolation analysis of thin walled wave barriers in poroelastic soils. *Computers and Geotechnics*, **71**, 168–179, 2016.

[14] J. Domínguez and M.P. Ariza, R. Gallego, Flux and traction boundary elements without hypersingular or strongly singular integrals. *International Journal for Numerical Methods in Engineering*, **48**, 111–135, 2000.

[15] A. Portela, M.H. Aliabadi, D.P. Rooke, The Dual Boundary Element Method: effective implementation for crack problems. *International Journal for Numerical Methods in Engineering*, **33**, 1269–1287, 1992.

[16] Y. Mi, M.H. Aliabadi, Dual Boundary Element Method for three-dimensional fracture mechanics analysis. *Engineering Analysis with Boundary Elements*, **10**, 161–171, 1992.

[17] E. Oñate, *Structural Analysis with the Finite Element Method. Linear Statics. Volume 2: Beams, Plates and Shells*. Lecture notes on Numerical Methods in Engineering and Sciences. CIMNE - Springer, 2013.

[18] J.L. Buchanan, R.P. Gilbert, Transmission Loss in the Far Field over a One-layer Seabed assuming the Biot sediment model. *Journal of Applied Mathematics & Mechanics*, **2**, 121–135, 1997.